Cancer Immunology, Immunotherapy (2025) 74:162
https://doi.org/10.1007/s00262-025-04002-6

RESEARCH

RNF2 induces myeloid-derived suppressor cells chemotaxis and promotes hepatocellular carcinoma progression through the TRAF2-NF-κB signaling axis

Manman Liang[1,2] · Jianghua Yang[2] · Aiping Zhang[2] · Na Zhong[3] · Bin Quan[2] · Zijian Wang[2] · Wenying Zhao[3] · Biao Geng[4] · Yufeng Gao[1]

Received: 1 November 2024 / Accepted: 26 February 2025 / Published online: 27 March 2025

Abstract

RING finger protein 2 (RNF2) has been shown to promote tumor growth in various cancer types. However, the immune regulatory function of RNF2 in the tumor microenvironment is unclear. Here, we report that upregulation of RNF2 is positively correlated with the tumor burden and poor prognosis in hepatocellular carcinoma patients and fosters an immunosuppressive microenvironment with increased MDSCs recruitment, and reduced T cell activation. Mechanistically, RNF2 binds with TRAF2 and directly mediates K63-linked TRAF2 ubiquitination. This modification of TRAF2 enables NF-κB hyperactivation in tumor cells, which subsequently induces CXCL1 transcription to enhance MDSCs migration. Furthermore, RNF2 knockout improves responsiveness to anti-PD-1 therapy in immunocompetent mice, as evidenced by enhancing infiltration of $CD8^+$T cells into the tumor and a reduction in MDSC levels. Collectively, our experiments support that perturbing RNF2 and targeting MDSCs may afford therapeutic opportunities for hepatocellular carcinoma interception and prevention.

Keywords RNF2 · TRAF2 · NF-κB · MDSC · HCC

Abbreviations

Arg1	Arginase-1
HCC	Hepatocellular carcinoma
IHC	Immunohistochemistry
iNOS	Inducible nitric oxide synthase
MDSCs	Myeloid-derived suppressor cells
NF-κB	Nuclear factor κB
PLA	Proximity ligation assay
RNF2	RING finger protein 2
TRAF2	Tumor necrosis factor receptor-associated factor 2
TIMER2.0	Tumor Immune Estimation Resource 2.0

Manman Liang and Jianghua Yang have contributed equally to this work.

✉ Biao Geng
wnyxy1@163.com

✉ Yufeng Gao
gaoyufeng0917@126.com

[1] Department of Infectious Diseases, The First Affiliated Hospital of Anhui Medical University, Hefei 230022, China

[2] Department of Infectious Diseases, Yijishan Hospital, The First Affiliated Hospital of Wannan Medical College, Wuhu 241000, Anhui, China

[3] Department of Medical Oncology, Yijishan Hospital, The First Affiliated Hospital of Wannan Medical College, 2 Zheshan West Road, Wuhu 241000, Anhui, China

[4] Department of Respiratory Medicine, Yijishan Hospital, The First Affiliated Hospital of Wannan Medical College, Wuhu 241000, Anhui, China

Hepatocellular carcinoma (HCC) is the most common major type of primary liver cancer and has a strikingly high mortality rate in China. Immune evasion is a hallmark of cancer. Therapies to enhance anti-tumor immune response, particularly antibodies blocking inhibitory immune checkpoint proteins such as programmed cell death protein 1 (PD-1), have achieved clinical success in the management of various cancers including advanced HCC. However, anti-PD-1 monotherapy induces lasting responses in only a subset of patients, with some eventually relapsing after an initial positive response 1, 2. Therefore, a deeper understanding of the mechanisms driving resistance to anti-tumor immune responses could improve clinical outcomes for HCC patients.

Myeloid cells, essential components of the tumor microenvironment, contribute to all stages of tumor progression.

Emerging evidence suggests that myeloid-derived suppressor cells (MDSCs) play a pivotal role in cancer immune evasion by suppressing T cell anti-tumor activity and modulating innate immune responses3. High levels of MDSC infiltration promote immune evasion by inhibiting the function of T cells and natural killer (NK) cells 4. MDSCs can be classified into two main sub-populations: monocytic MDSCs (M-MDSCs) and polymorphonuclear (PMN)-MDSCs, also known as granulocytic MDSCs (G-MDSCs)4. These subsets exhibit differences in gene expression profiles and immunosuppressive functions. In many cancers, including HCC, the abundance of MDSCs correlates with disease stage and metastatic burden5. However, the factors driving MDSC subset accumulation and their specific roles in HCC development remain underexplored 4, 5. While gene alterations in cancer cells are known to contribute to localized MDSC expansion, the signaling pathways governing the HCC immunosuppressive tumor microenvironment are largely unclear6.

HCC is characterized by a highly inflammatory tumor microenvironment. The nuclear factor κB (NF-κB) pathway is crucial for linking inflammation and cancer, promoting tumor growth, and conferring resistance to therapy 7. Aberrant NF-κB activation has been observed in various cancers, including HCC and colorectal cancer 7, 8. Consequently, inhibiting NF-κB is considered a promising strategy for enhancing anti-cancer therapies by altering the gene expression profile associated with NF-κB signaling. A recent breakthrough revealed that the classical NF-κB subunit, cRel, supports immunosuppression by maintaining activated tumor-infiltrating regulatory T cells (Tregs), which inhibit the function of anti-tumor CD8 + effector T cells9. Interestingly, both the classical and alternative NF-κB pathways have been identified as promising molecular targets for boosting the anti-tumor efficacy of checkpoint inhibitors. In murine xenograft models of melanoma and colorectal cancer, combining anti-PD-1 therapy with NF-κB pathway inhibition resulted in complete and lasting anti-tumor responses, which were not observed with either treatment alone 9–11. Nevertheless, the molecular mechanisms by which the NF-κB pathway interacts with immune cells to modulate HCC tumorigenesis remain largely unknown.

In this study, we discovered that RNF2 expression is positively correlated with tumor burden and poor prognosis in HCC patients. The upregulation of RNF2 contributes to the development of a pro-tumorigenic microenvironment, primarily characterized by increased recruitment of MDSCs and reduced T cell activation, through its regulation of NF-κB pathway activation. Mechanistically, RNF2 interacted with TRAF2, promoting K63-linked polyubiquitination of TRAF2 and subsequent activation of the NF-κB signaling pathway, which in turn facilitated MDSC migration via the CXCL1-CXCR2 axis. The accumulation of MDSCs further antagonized the function of $CD8^+$T cells within the tumor immune microenvironment. Collectively, our findings suggest that targeting RNF2 may offer a novel therapeutic strategy for attenuating tumor progression and immune evasion in HCC.

Materials and methods

Cell lines and cell culture

Murine HCC cell line H22, Hepa1–6, LM3 and human HCC cell line HepG2, HuH7, Sk-Hep1, Hep3B, SMMC-7721 were purchased from the Cell Bank of Type Culture Collection of the Chinese Academy of Sciences Shanghai Institute of Biochemistry and Cell Biology with STR (short tandem repeat) appraisal certificates. All cell lines were tested negative for mycoplasma contamination. Human embryonic kidney 293 T cells were purchased from the American Type Culture Collection (ATCC) and maintained in our laboratory. Cells were maintained in Dulbecco's modified Eagle medium supplemented with 10% fetal bovine serum at 37 °C in 5% CO2.

Western blot and immunoprecipitation assays

For western blot analysis, cells or fresh tissues were lysed on ice using RIPA buffer supplemented with protease and phosphatase inhibitors (Roche). Protein extracts were clarified, and concentrations were measured with Pierce Protein Assay kit. Western blot procedure was performed as previously described12. Protein lysates were mixed with SDS-PAGE loading dye and then subjected to SDS-PAGE for immunoblotting. The following antibodies were used for immunoblots: RNF2 (Cat: A302-869A-T, Invitrogen), TRAF2 (Cat: PA5-20,192, Invitrogen), Phospho-IκBα (Cat: #2859, Cell Signaling Technology), IκBα (Cat: #4814, Cell Signaling Technology), Phospho-IKKα/β (Cat: #2697, Cell Signaling Technology), IKKα (Cat: #2682, Cell Signaling Technology), IKKβ (Cat: #8943, Cell Signaling Technology), anti-flag (Cat: #14,793, Cell Signaling Technology), anti-ubiquitin (Cat: #3936, Cell Signaling Technology), anti-K48-linkage specific polyubiquitin (Cat: #8081, Cell Signaling Technology), and anti-K63-linkage specific polyubiquitin (Cat: #5621, Cell Signaling Technology).

Primary antibodies were added and incubated overnight at 4 °C with rotation. Protein G beads were added and incubated for 3 h at 4 °C with rotation. The resin was centrifuged, washed three times with lysis buffer, and analyzed by immunoblotting.

Plasmid constructs and RNA interference

Human HA-RNF2, Flag-TRAF2 (Cat: HG16513-NF) expression plasmid, human RNF2 lentiviral particles (Cat: HG18649-ACGLN), and mouse RNF2 lentiviral particles (Cat: MG57998-ACGLN) were purchased from Sino Biological Inc. Scrambled, human RNF2 short hairpin RNAs (shRNAs) was obtained from Shanghai Genechem Co., Ltd. (Shanghai, China). RNF2 Knockout Lentivirus (Cat: L10426) and Control Knockout Lentivirus (L00015) were purchased from Beyotime Biotechnology. Upon verification, knockout of RNF2 in mouse liver cancer cells does not induce immunogenic cell death (Supplementary Fig. 1).

To elucidate the role of RNF2 as an E3 ligase, we generated an E3 ligase-defective RNF2 by using the KOD-Plus-Mutagenesis kit (Toyobo, cat: SMK-101) and verified by performing DNA sequencing. Plasmid transfection was performed using the Lipofectamine 3000 transfection reagent (Thermo Fisher, Cat#L3000015) according to the manufacturer's instructions. After 48 h, biological and biochemical experiments were performed.

Reverse transcription quantitative PCR (RT-qPCR) analysis

Total RNA was extracted from tumor or normal tissues or cells using TRIzol reagent (Invitrogen), and cDNA synthesis using the Prime-Script cDNA synthesis kits (Invitrogen) according to the manufacturer's instructions. The reverse-transcribed cDNA products were used for qPCR analysis using SYBR Green PCR kit (Invitrogen). The value obtained for each gene was normalized to that of the gene encoding GAPDH. Human (Cat: HP100763) and mouse (Cat: MP200180) CXCL1 and human GAPDH (Cat: HP100003) and mouse GAPDH (Cat:MP200537) qPCR Primer Pair were purchased from Sino Biological Inc.

Multiplexed immunofluorescent staining

These experiments were performed as previously described12. For multiplexed immunofluorescent staining, Opal 4-color fluorescent IHC kit (Akoya Biosciences, Cat: #NEL810001KT) was used. First, the concentration and the application order of the three antibodies were optimized, and the spectral library was built based on the single-stained slides. The slides were first deparaffinized by xylene and ethanol, and antigen retrieval was performed by microwave. After incubating with 3% H2O2 (freshly made) for 10 min, the tissues were blocked in blocking buffer for another 10 min at room temperature. Then the tissues were incubated by primary antibody, secondary-HRP (Cell Signaling Technology) and Opal working solution (Akoya Biosciences). The slides then were mounted with ProLong Gold Antifade Reagent with DAPI and were scanned using confocal microscopy.

Immunofluorescence confocal imaging

Cells were grown on Lab-Tek chamber slides, fixed with 4% paraformaldehyde in PBS for 30 min, and permeabilized with 0.1% Triton X-100 in PBS for 5 min. The slides were incubated with primary antibodies in blocking solution overnight at 4 °C in a humidified chamber. Subsequently, the glass slides were washed three times in PBS and incubated with Alexa Fluor 594-conjugated and Alexa Fluor 488-conjugated secondary antibodies and 4, 6-diamidino-2-phenylindole (DAPI) in blocking solution for 30 min at 37 °C in a humidified chamber. Images were acquired with a Leica confocal system.

Ubiquitination assay

The experiments were performed as previously described 12. In summary, 293 T cells were transfected with his-ubiquitin along with other specified plasmids for 36 h. Post-transfection, the cells were harvested using denaturing buffer A, which consists of 6 M guanidine-HCl, 0.1 M Na_2HPO_4/NaH_2PO_4, and 10 mM imidazole at pH 8. To isolate his-ubiquitin and its conjugated proteins, pre-washed Ni–NTA Agarose beads (QIAGEN) were incubated with the cell lysates for 3.5 h. After incubation, the beads underwent washing with buffer A and buffer T1 (containing 25 mM Tris–Cl and 20 mM imidazole at pH 6.8) before being analyzed via western blotting.

Immunohistochemistry (IHC) staining and scoring

We enrolled 90 patients diagnosed with HCC at the First Affiliated Hospital of Wannan Medical College for the retrospective study. Formalin-Fixed and Paraffin-Embedded (FFPE) tumor tissues were retrospectively obtained from HCC patients with available clinicopathological features and complete follow-up data was performed who received surgically treated from January 2015 to December 2020. The Medical Ethics Committee of The First Affiliated Hospital of Wannan Medical College approved the collection of samples and medical records. After deparaffinization with xylene, paraffin sections were rehydrated. Tissue sections were filled with EDTA for antigen retrieval and

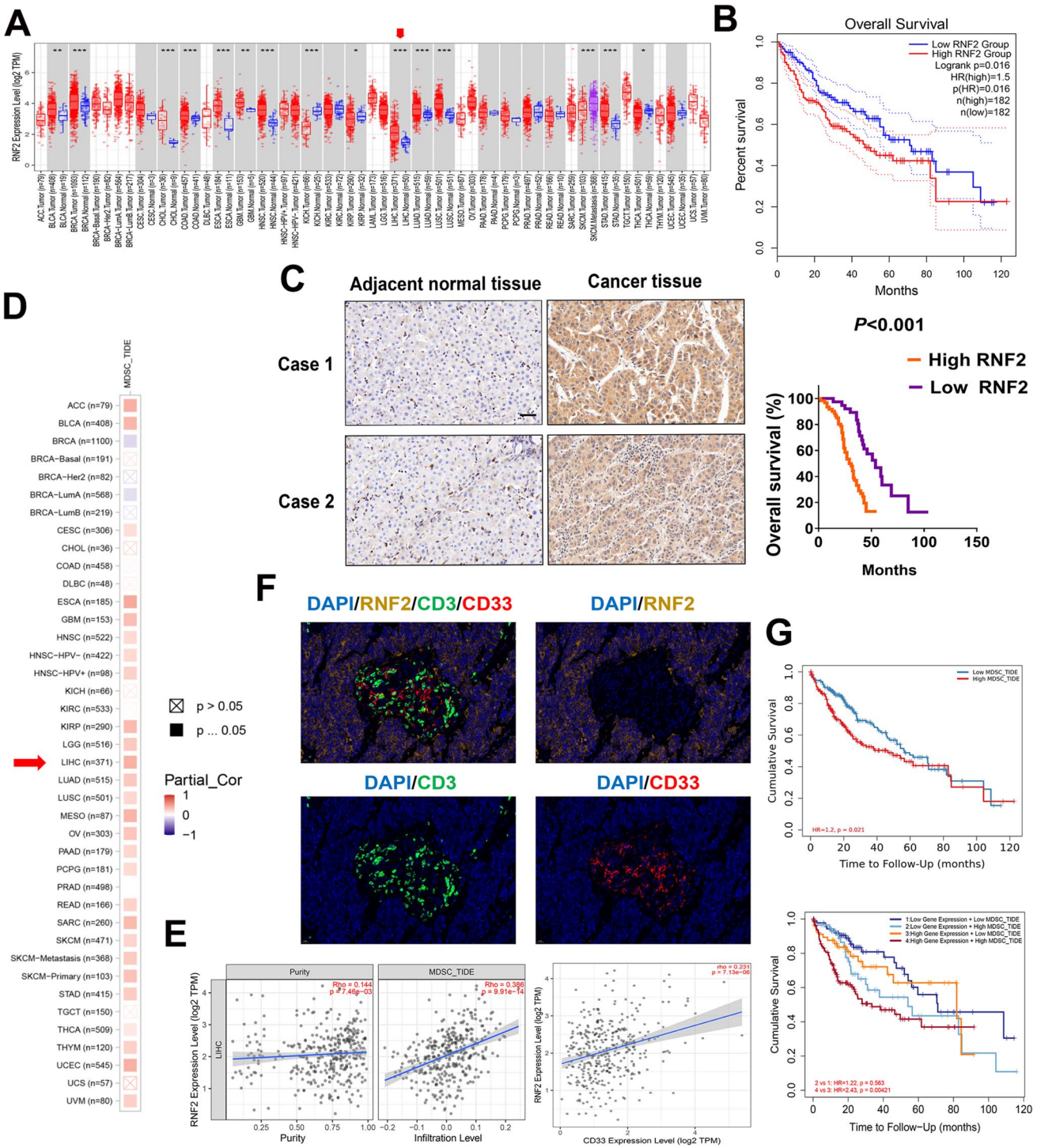

treated with 3% H2O2 solution for 15 min at room temperature to block endogenous peroxidase activity. After blocking with 10% goat serum for 30 min at room temperature, slides were incubated with primary antibodies at 4 °C overnight. The following antibodies were used: RNF2 (Cat: PA5-27,648, Invitrogen), CXCL1(Cat:PA5-86,508, Invitrogen), anti-CD8(Cat: ab237723, abcam), and anti-S100A8 + S100A9 (Cat: ab288715, abcam). After cleaning, the tissues were incubated with secondary antibodies at room temperature for 50 min. The tissues were initially stained with a diaminobenzidine (DAB) color developing solution, followed by counterstaining with haematoxylin stain solution, dehydration, and coverslip sealing.

The staining intensity scores were evaluated as 0 (negative staining), 1 (slight staining), 2 (moderate staining),

◂**Fig. 1** RNF2 positively correlates with progression and poor prognosis of HCC by recruiting MDSCs into the tumor microenvironment. **A** Comparison of RNF2 expression between tumor and normal tissues from TCGA database analyzed by TIMER 2.0. **B** K-M analysis of the OS of HCC patients in the TCGA liver hepatocellular carcinoma (LIHC)cohort based on the expression level of RNF2. Data were analyzed by log-rank test. **C** Representative images of IHC staining of RNF2. Scale bars: 100 μm (black). Patients were divided into two groups based on RNF2 expression levels. The low expression group consisted of patients exhibiting negative or weak RNF2 expression, while the high expression group included those with moderate to strong expression. Overall survival curves were generated using the log-rank test to assess differences in survival rates between the two groups. (D-E) The expression of RNF2 was positively correlated with the infiltration levels of MDSCs in LIHC analyzed by TIMER 2.0. Correlation analysis indicated that RNF2 expression was positively correlated with CD33 expression. **F** Representative mIHC staining of CD33 and RNF2 in tissue from human HCC tumors. Multiplexed immunofluorescence staining images showing the expression of RNF2, CD8, CD33 and DAPI in HCC. **G** High infiltration levels of MDSCs were associated with poor survival. Cox regression analysis of TCGA data demonstrated a significant correlation between increased MDSC infiltration and worse prognosis in HCC patients. Furthermore, elevated RNF2 expression and a high proportion of MDSCs significantly correlated to poorer OS compared to their counterparts, strongly suggesting that RNF2 influenced patient prognosis through an immune-related mechanism

and 3 (strong staining). The percentage of positive cells was scored as 0 (< 10%), 1 (10–25%), 2 (25–50%), and 3 (> 50%). Specimens with final scores ≥ 2 were considered to have high expression, while those with final scores < 2 were considered to have low expression. For immune cell markers where signal intensity was not considered, the percent positive cell score was calculated based on the percentage of positively stained cells.

Enzyme-linked immunosorbent assay (ELISA)

ELISA against murine and human CXCL1 were both acquired from Abcam and used according to the user manuals. Supernatant samples collected from in vitro cell culture were used without dilution, while tumor lysates and sera were used after dilution of five times prior to assessment.

Immune infiltration analysis

Tumor Immune Estimation Resource 2.0 (TIMER2.0) is a comprehensive web server (http://timer.cistrome.org/) for analyzing immune infiltrates across diverse cancer types13. It integrates various immune estimation algorithms, including TIMER13, CIBERSORT14, quanTIseq15, xCell16, MCP-counter17, EPIC18. For example, xCell (https://xcell.ucsf.edu/) calculates enrichment fractions of cell type signatures in bulk RNA data using the GSEA algorithm, converts them to cell type fractions, and adjusts for closely related cell types, yielding semi-quantitative scores linearly correlated with true cell proportions. Similarly, CIBERSORT (https://cibersortx.stanford.edu/) characterizes expression data of 22 common immune infiltrating cells to form LM22 reference files and then deconvolutes uploaded expression matrices to estimate immune cell abundance using linear support vector regression.

MDSC isolation and migration assay

MDSCs were isolated from the spleens of Hepa1-6 tumor-bearing C57BL/6 mice using EasySep Mouse MDSC ($CD11b^+Gr1^+$) Isolation Kit (STEMCELL). MDSCs (1×10^5cells/well) were seeded in the top chamber of the transwell (Corning). Conditioned media from cultured Hepa1-6 cell lines (with or without RNF2 knockout; with or without SX-682 or CXCL1 antibody pretreatment) were collected and added to the bottom layer of the transwell. After 4-h incubation, cells that migrated to the bottom chamber were counted.

Flow cytometry and lymphocyte staining

Tissues were dissected, minced into small pieces and further digested by 1 mg/ml Collagenase Type II (Thermo Fisher Scientific), 1 mg/ml Collagenase Type IV (Thermo Fisher Scientific) and 0.1 mg/ml DNase I recombinant (Sigma-Aldrich) at 37 °C for 30–60 min. The single-cell suspensions of tumor-burdened livers were resuspended in FACS buffer (PBS, 1%BSA) and blocked with anti-mouse CD16/32 antibodies for 10 min prior to staining with the antibodies of the surface markers. For intracellular cytokine staining, cells were fixed and permealized with a fixation and permeabilization solution kit (Biolegend) followed by staining with the specific antibodies against intracellular cytokines. The following antibodies were acquired from Biolegend and used in the flow cytometry analysis: BV605 anti-mouse CD45 (clone 30-F11), PE anti-mouse CD3 (clone 17A2), PE/Cy7 anti-mouse CD4 (clone RM4-5), BV711 anti-mouse CD8α (clone 53 – 6.7), BV421 anti-mouse Ly-6 C (clone HK1.4), PE anti-mouse Gr1 (clone RB6-8C5), PE/Cy5 anti-mouse CD11b (clone M1/70), PE/Cy7 anti-mouse Ly-6G (clone 1A8), BV711 anti-mouse IFN-γ (clone XMG1.2), BV421 anti-mouse CD8α (clone 53 – 6.7), PE/Cy5 anti-mouse CD3 (clone 17A2). Flow cytometry data were acquired on

a FACS Celesta flow cytometer and data were analyzed with FlowJo V10.

Luciferase assays

Cells were cultured in 12-well plates and then transiently transfected with NF-κB luciferase reporter plasmid (1 μg) and Renilla plasmid (100 ng). At 48 h post-transfection, luciferase activities were measured using the Dual-Luciferase Reporter Assay System (Promega) according to the manufacturer's protocols.

T cell suppression assay

MDSCs were isolated from tumor-bearing livers using EasySep™ Mouse MDSC (CD11b + Gr1 +) Isolation Kit (STEMCELL). Autologous spleen was used for T cells isolation by EasySep Mouse T Cell Isolation Kit (STEMCELL), and then isolated T cells were labeled with carboxyfluorescein succinimidyl ester (CFSE) (Invitrogen). CFSE-labeled T cells were cocultured with MDSC cells at 96-well plates (T: MDSC = 1:1) for 72 h, Dynabeads Mouse T Activator CD3/CD28 (ThermoFisher), and IL-2 (BioLegend) was added into medium for culture. CFSE intensity was quantified by flow cytometry.

Animal experiments

Orthotopic HCC model was established by intrahepatic implanting 1×10^6 Hepa1-6 transduced cells into the liver. Two weeks later, mice were killed and the tumor tissues were harvest for future experiments. Another orthotopic model was established by tail vein injection. In brief, 1×10^6 Hepa1-6 transduced cells resuspended in 2.5 mL PBS were injected into the tail vein. Three weeks later, mice were killed, and the tumor nodules were counted. For the drug treatment subcutaneous tumor models, 1×10^6 Hepa1-6 cells were injected subcutaneously into syngeneic wild-type C57BL/6 male mice. Tumors formed until volumes were ~ 150-200mm^3 as measured by digital calipers before treatments were administered. Mice were treated weekly with 200 μg of anti-mouse PD-1 mAb (BE0146, Bio X cell) by intraperitoneal injection. Control mice received 200 μg of isotype control (Bio X Cell). All animal experiments were approved by the Institutional Animal Care and Use Committee of Yijishan Hospital.

Statistical analysis

GraphPad Prism v9 was used to draw graphs and perform statistical tests. To determine the significance of observed differences, log-rank test, Student's t-test, and one-way analysis of variance with Tukey's multiple comparison test were employed. Comparisons with $p < 0.05$ were considered to be statistically significant.

Results

RNF2 is overexpressed and positively correlated with MDSCs in HCC

To determine the clinical significance of RNF2 expression, we analyzed RNA sequencing data from the Cancer Genome Atlas (TCGA). Our analysis showed that RNF2 mRNA levels were significantly elevated in various tumor types compared to normal tissues (Fig. 1A). Specifically, RNF2 expression was markedly higher in hepatocellular carcinoma tissues than in non-tumorous samples. Moreover, high levels of RNF2 expression were strongly associated with poor prognosis in HCC patients (Fig. 1B).

To further explore the relationship between RNF2 and tumor progression, as well as its prognostic value in HCC, we performed immunohistochemical staining for RNF2 on an HCC tissue microarray cohort. The staining results indicated that RNF2 expression was substantially higher in tumor tissues compared to adjacent non-tumor tissues (Fig. 1C). Importantly, elevated expression levels of RNF2 exhibited a positive correlation with a more aggressive tumor phenotype in HCC patients (Supplementary Table 1). Additionally, Kaplan–Meier survival analysis confirmed that increased RNF2 expression was associated with unfavorable prognoses for HCC patients (Fig. 1C). Altogether, these findings provide strong evidence of a positive correlation between RNF2 expression and tumor progression in HCC.

Genetic aberrations in tumors can regulate critical cellular processes such as the cell cycle, apoptosis, migration, and survival. Notably, a growing body of clinical evidence suggests that dysregulated oncogenic pathways in human cancers are also linked to alterations in immune cell composition and responses to immunotherapy6. As RNF2 closely correlates with the oncogenesis and metastasis of various cancers, we then further investigated whether RNF2 expression affects the immune landscape of the tumor through correlation analysis using the TIMER2.0 database. As expected, TIMER2.0 analysis revealed a positive association between RNF2 expression and MDSC infiltration across multiple cancer types (Fig. 1D). MDSCs in cancer patients have been

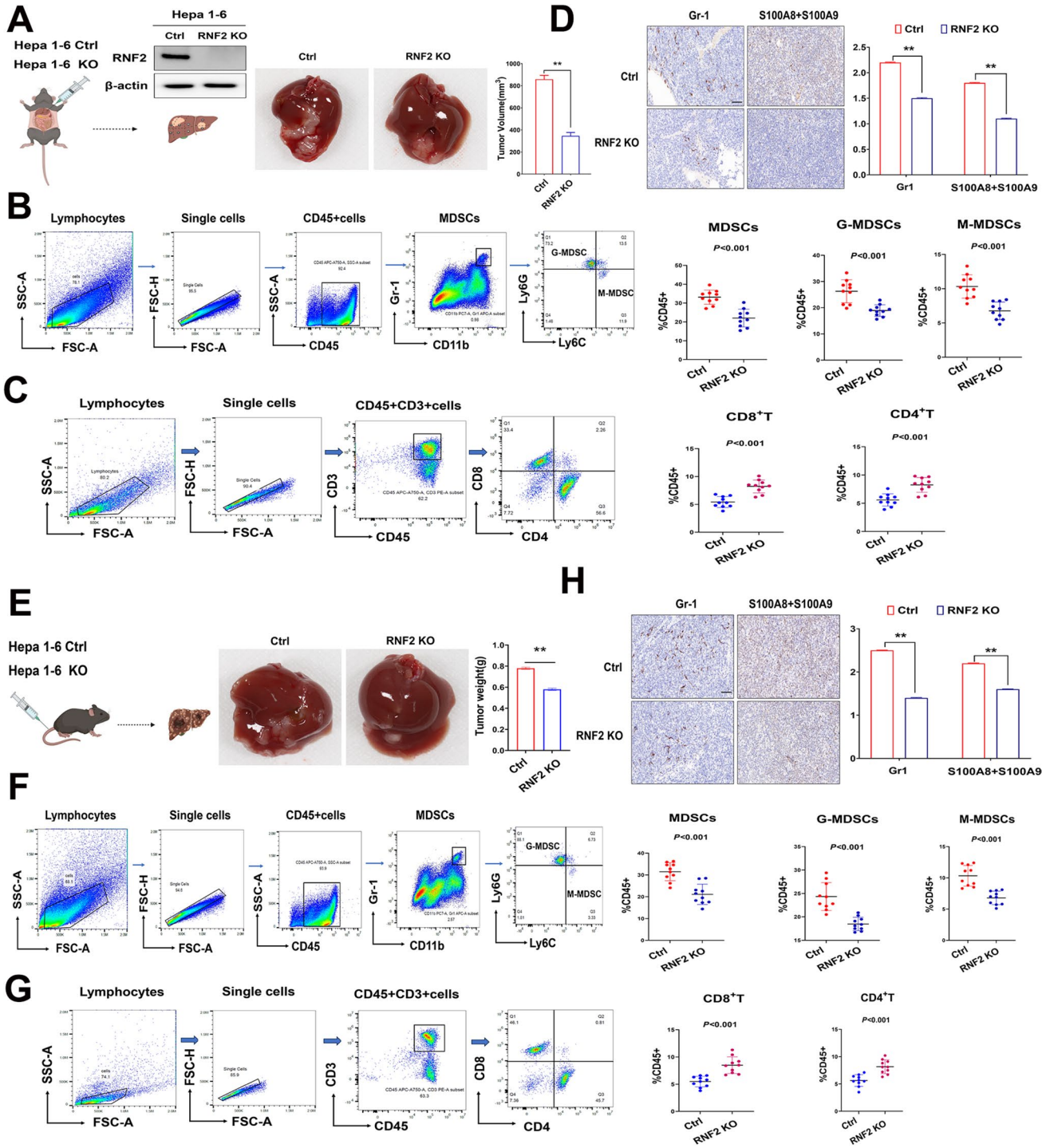

Fig. 2 RNF2 promoted HCC growth in murine orthotopic HCC models **A** Hepa1-6-Ctrl or Hepa1-6-RNF2 KO cells (1×10^6) were resuspended in 15 mL PBS and injected into the hepatic lobule via syringe. Two weeks later, mice were killed, and tumor weight was measured. (B-C) Tumors from Hepa1-6-Ctrl and Hepa1-6-RNF2 KO groups were analyzed for immune cell infiltration. The percentages of tumor-infiltrating MDSCs, CD4+, and CD8+T cells, gated on the CD45+population, are shown with representative flow cytometry plots. **D** Representative IHC images showing staining for MDSC markers (Gr1, S100A8, and S100A9) in orthotopic HCC models. The right panel displays quantification of MDSCs based on IHC analysis. **E** Hepa1-6-Ctrl or Hepa1-6-RNF2 KO cells (1×10^6) resuspended in 2.5 mL PBS were injected via the tail vein. Three weeks post-injection, mice were killed, and the weight of tumor-burdened livers was compared between the Hepa1-6-Ctrl and Hepa1-6-RNF2 KO groups. (F-G) Flow cytometric analysis of tumor-infiltrating MDSCs, CD4+, and CD8+T cells, gated on the CD45+population, with representative plots from the indicated tumor models. **H** IHC analysis for MDSCs markers. Scale bars, 100 μm. The right graph shows the quantification of MDSCs as analyzed by IHC. Significant differences between two groups and among multiple groups were analyzed by t-test and ANOVA, respectively. **p < 0.01

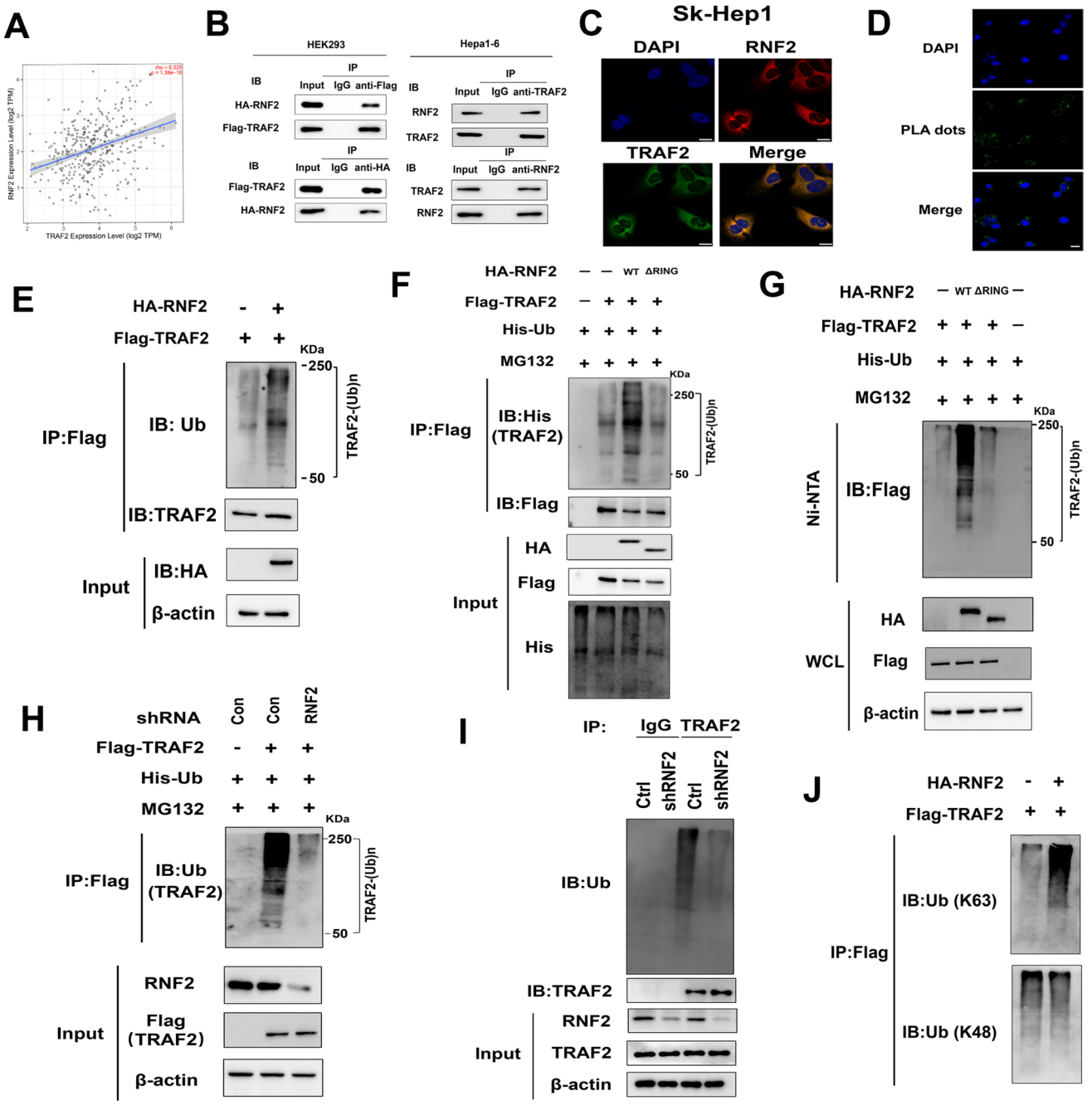

characterized by the expression of CD14, CD11b, CD33, and Arg1 and low or absent expression of HLA-DR6. This was supported by analysis of data in the TCGA database showing a positive correlation between RNF2 and CD33 mRNA in human HCC (Fig. 1E). While analyzing the tumor microenvironment of RNF2 high expressing tumors from patients with HCC, we noted an increase in CD33 + cells (Fig. 1F). These findings suggest that RNF2 plays a role in shaping the immune landscape of tumors by promoting MDSC infiltration, potentially influencing tumor progression.

By utilizing TIMER2.0, we further investigated the relationship between MDSC levels and overall survival (OS) in HCC patients, categorizing them based on high or low RNF2 expression. Elevated MDSC infiltration in tumor tissues was significantly associated with poor prognosis in HCC patients (Fig. 1G). Notably, among patients with low RNF2 expression, there was no significant difference in OS between those with low and high MDSC infiltration. In contrast, patients with high RNF2 expression and increased MDSC levels experienced worse survival outcomes, indicating that elevated RNF2 may enhance

◂**Fig. 3 RNF2 is required for K63-linked ubiquitination of TRAF2** **A** Correlation analysis between RNF2 and TRAF2 expression using TIMER 2.0. RNF2 expression positively correlates with TRAF2 levels in LIHC samples. **B** HEK-293 cells were transfected with HA-tagged RNF2 and Flag-tagged TRAF2. Lysates were prepared and immunoprecipitated using anti-HA or anti-Flag antibodies. Immunoblot analysis was performed as indicated. Immunoprecipitation assay further confirmed the interaction between endogenous RNF2 and TRAF2 in Hepa1-6 cells. **C** Immunofluorescence demonstrating co-localization of RNF2 and TRAF2 in Sk-Hep1 cells. **D** HEK-293 cells were transiently transfected with HA-tagged RNF2 and Flag-tagged TRAF2. Rabbit anti-HA and mouse anti-Flag antibody were used for the proximity ligation assay. Red dots present the interaction of RNF2 with TRAF2. Scale bars, 20 μm. **E** HEK-293 cells were transfected with HA-RNF2 and Flag-TRAF2 as indicated. Cell lysates were immunoprecipitated with anti-Flag and immunoblotted with anti-ubiquitin, anti-TRAF2, or anti-HA as indicated. (F and G) RAF2 ubiquitination increased upon overexpression of wild-type RNF2 (RNF2-WT), but not the ΔR mutant. 293 T cells were transfected with HA-RNF2-WT or ΔR mutant. Lysates were subjected to immunoprecipitation with anti-Flag antibodies **F** or Ni–NTA pull-down under denaturing conditions **G**, followed by immunoblotting with the indicated antibodies. **H** TRAF2 ubiquitination decreased after RNF2 depletion. 293 T cells were co-transfected with the indicated plasmids or shRNAs. Immunoprecipitation of Flag-TRAF2 followed by immunoblot analysis was performed. **I** Sk-Hep1 cells transfected with control or RNF2 shRNA. Endogenous TRAF2 was immunoprecipitated and analyzed for ubiquitination. **G** RNF2 mediates K63-linked ubiquitination of TRAF2. Lysates from **E** were immunoprecipitated with anti-Flag antibodies and immunoblotted with antibodies against K63- and K48-linked ubiquitin

the immunosuppressive effects of MDSCs (Fig. 1G). These findings highlight a strong connection between RNF2 expression and the presence of immunosuppressive MDSCs in cancer. In summary, RNF2 is highly expressed in HCC tumor tissues and positively correlates with MDSC infiltration in the tumor microenvironment, likely contributing to accelerated tumor progression.

RNF2 deficiency in tumor cells inhibits tumor growth by inhibiting tumor-infiltrating MDSCs

We aimed to investigate how the deficiency of RNF2 in tumor cells affects the immune microenvironment of transplanted tumors. To assess the role of Hepa1-6 cells in tumor growth, we generated an RNF2 knockout (RNF2 KO) Hepa1-6 cell line, as Hepa1-6 cells have a high expression level of RNF2, by transducing the cells with an RNF2 knockout lentivirus (Fig. 1A and Supplementary Fig. 2A). We compared their tumorigenic ability to control cells transduced with a control knockout lentivirus (Ctrl). Subsequently, we established an orthotopic HCC model by surgically implanting either Hepa1-6-Ctrl or Hepa1-6-RNF2 KO cells into the livers of syngeneic wild-type mice. The tumors formed by RNF2 KO cells were significantly smaller in size and area compared to those in the control group (Fig. 2A).

To determine whether tumor-derived RNF2 affects the accumulation and function of MDSCs in the tumor microenvironment, we analyzed the number of intratumoral MDSCs using flow cytometry and immunohistochemistry. Flow cytometry results showed that both the percentage and absolute number of MDSCs were significantly lower in RNF2 KO tumors compared to control tumors (Fig. 2B). It is noteworthy that a higher abundance of tumoral MDSCs is significantly correlated with increased tumor burden and reduced infiltration and activation of T cells 6. Interestingly, RNF2 KO tumors exhibited higher infiltration of $CD4^+$ and $CD8^+$ T cells compared to control tumors (Fig. 2C). These findings were further corroborated by immunohistochemistry staining, which revealed a marked reduction in MDSC numbers and significantly lower expression levels of CD11, S100A8, and S100A9 in RNF2 KO tumors compared to controls (Fig. 2D).

To validate our observations, we established another murine orthotopic HCC model by injecting Ctrl or RNF2 KO cells via the tail vein. Consistent with previous results, the weight of tumor-bearing livers was significantly reduced in the RNF2 KO group compared to the control group (Fig. 2E). Additionally, both the numbers and percentages of MDSCs were markedly lower in the tumor-bearing livers of mice in the RNF2 KO group compared to controls (Figs. 2F-2H). Furthermore, the proportions of $CD4^+$ and $CD8^+$ T cells were elevated in RNF2 KO tumors (Fig. 2G). These results suggest that RNF2 promotes MDSC accumulation in the tumor microenvironment, highlighting a significant link between RNF2 expression and MDSC infiltration in HCC.

E3 Ligase RNF2 targets TRAF2 for K63-linked ubiquitination

To elucidate the molecular mechanisms by which RNF2 promotes HCC progression, we conducted in-depth bioinformatics analysis of mass spectrometry data, identifying the oncoprotein RNF2 as a potential interactor of TNF receptor-associated factor 2 (TRAF2)19. Using TIMER2.0 analysis, we further identified a positive correlation between RNF2 and TRAF2 expression in HCC (Fig. 3A). TRAF2 is an oncogenic protein that contributes to NF-κB-mediated resistance to TNF-induced apoptosis in cancer cells. As illustrated in Fig. 3B, co-immunoprecipitation assays showed that exogenous RNF2 interacts with TRAF2 in HEK-293T cells co-transfected with HA-RNF2 and Flag-TRAF2 plasmids. Similarly, the same interaction was observed between endogenous RNF2 and TRAF2 in Hepa1-6 cells. Additionally, confocal microscopy analysis demonstrated that RNF2 predominantly co-localizes with TRAF2 in Sk-Hep1 cells

(Fig. 3C). We also employed a proximity ligation assay, which generates a spatial fluorescent signal within a maximum distance of 30–40 nm, thereby confirming close proximity interactions between protein partners. As shown in Fig. 3D, RNF2 is robustly detected in proximity to TRAF2 in Sk-Hep1 cells. Collectively, these studies establish that RNF2 physically associates with TRAF2.

The stability of TRAF2 is governed by intricate post-translational modifications and its interactions with other signaling proteins within the signalosome20. To explore whether RNF2 acts as an E3 ubiquitin ligase for TRAF2, we co-transfected HEK-293T cells with Flag-TRAF2 and either HA-RNF2 or control plasmids, followed by immunoblot analysis to evaluate TRAF2 ubiquitination. We observed that Flag-TRAF2 ubiquitination was significantly enhanced in cells expressing RNF2 (Fig. 3E). Understanding that the RING finger domain is essential for E3 ligase enzymatic activity, we conducted immunoprecipitation of exogenous TRAF2 and performed nickel-nitrilotriacetic acid (Ni–NTA) pull-downs under denaturing conditions. The results showed a dramatic increase in TRAF2 ubiquitination when wild-type HA-RNF2 was overexpressed, but not with HA-RNF2-ΔRING—a mutant lacking the RING domain (Fig. 3F-3G). Moreover, silencing endogenous RNF2 in 293 T cells led to a decrease in Flag-TRAF2 ubiquitination (Fig. 3H). Consistent with RNF2's role in promoting TRAF2 ubiquitination, depletion of RNF2 significantly reduced the ubiquitination of endogenous TRAF2 in RNF2-depleted Sk-Hep1 cells (Fig. 3I and Supplementary Fig. 2B). These findings indicate that the E3 ligase activity of RNF2 is crucial for mediating TRAF2 ubiquitination.

Previous studies have reported that RNF2 can catalyze the attachment of both K48- and K63-linked ubiquitin chains by interacting with two distinct E2 ubiquitin-conjugating enzymes. To identify the specific type of ubiquitin chain RNF2 adds to TRAF2, we performed an in vivo ubiquitination assay. Immunoblot analysis revealed that overexpressing RNF2 increased K63-linked ubiquitination of endogenous TRAF2 without affecting K48-linked ubiquitination (Fig. 3J). Collectively, these findings demonstrate that RNF2 functions as an E3 ligase, specifically catalyzing K63-linked ubiquitination of TRAF2.

RNF2 promotes NF-κB signaling

It has been previously reported that the K63-linked polyubiquitin chains could be attached to TRAF2, necessary for the signalosome formation and NF-κB activation21. Our findings indicate that the E3 ligase activity of RNF2 is vital for mediating K63-linked ubiquitination of TRAF2, suggesting that RNF2 plays a significant role in activating the NF-κB signaling pathway. Additionally, RNF2 deficiency sensitizes liver cancer cells to TNF-α-induced apoptosis, indicating that RNF2 protects cells from TNF-α-induced cell death, likely through modulation of the NF-κB signaling pathway (Supplementary Fig. 3). Supporting this, luciferase assays showed increased activity of the NF-κB luciferase reporter gene in cells overexpressing wild-type RNF2 but not in those expressing the RNF2-ΔRING mutant (Fig. 4A). Conversely, inhibiting RNF2 reduced reporter activity, highlighting the necessity of its E3 ligase function for NF-κB activation (Fig. 4A). To further corroborate these results, we observed that silencing RNF2 significantly decreased the phosphorylation of IκBα and IKKα/β in Hepa1-6 and Sk-Hep1 cells (Fig. 4B). Additionally, we explored whether RNF2 facilitates sustained NF-κB activation by treating cells with TNF-α and measuring IκB protein levels. In RNF2-depleted cells, the reduction in IκB levels was transient, indicating a shorter duration of NF-κB activation (Fig. 4C). To further validate these findings, we blocked the NF-κB pathway by expressing an IκBα dominant-negative mutant (IκBα-mu) in cells overexpressing RNF2. As expected, the NF-κB activation induced by RNF2 overexpression was inhibited by IκBα-mu (Fig. 4D). These results suggest that RNF2 regulates NF-κB activation by enhancing K63-linked ubiquitination of TRAF2, thereby establishing its crucial role in modulating this key oncogenic signaling pathway.

RNF2 Promotes MDSC recruitment via NF-κB-CXCL1 axis

Prior studies have demonstrated that the NF-κB pathway activates CXCL1 transcription22. CXCL1, a chemotactic factor, recruits MDSCs into the tumor microenvironment by binding to its receptor CXCR222. Our study also found that in a syngeneic mouse tumor model, blocking CXCL1 with a monoclonal antibody significantly inhibits liver cancer growth (Supplementary Fig. 4). TCGA database analysis showed a positive correlation between RNF2 expression and CXCL1 levels in hepatocellular carcinoma tissues (Fig. 5A). Similarly, TRAF2 was also positively correlated with CXCL1. Based on these findings, we hypothesized that RNF2-mediated NF-κB pathway activation might be responsible for enhancing CXCL1 expression. To test this hypothesis, we analyzed nuclear phospho-p65 levels in liver cancer cell lines using western blotting. Phospho-p65, a key factor in the canonical NF-κB pathway, was decreased in RNF2-depleted cell lines (Fig. 5B). Immunofluorescence analysis further confirmed these results, showing a substantial reduction in nuclear phospho-p65 staining in RNF2-depleted Hepa1-6 and Sk-Hep1 cells compared to controls (Fig. 5C). Next, we assessed whether RNF2 alters CXCL1 expression in murine and human liver cancer cell lines. RT-qPCR confirmed that RNF2 deficiency suppressed CXCL1 mRNA

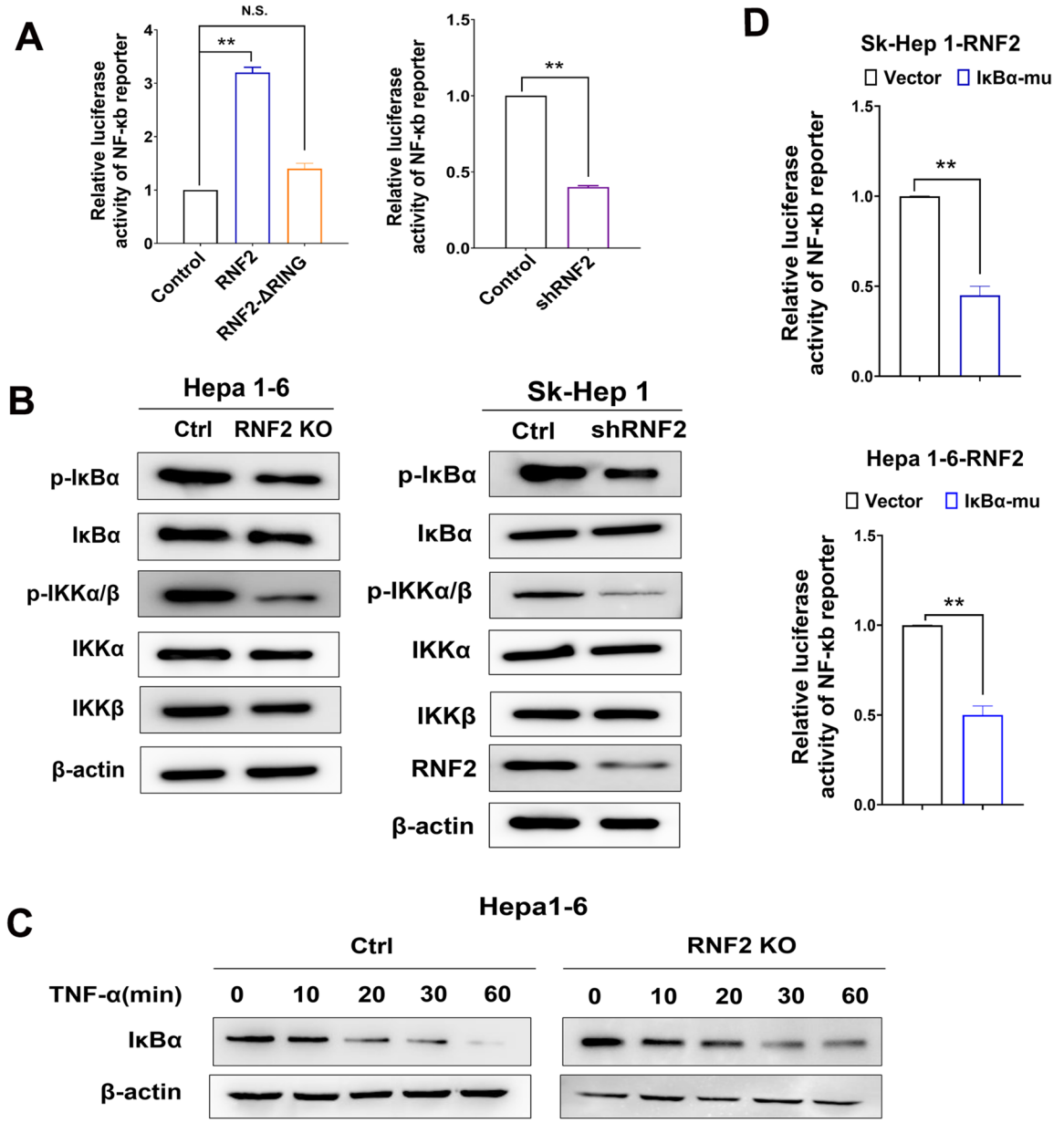

Fig. 4 RNF2 activates NF-κB signaling **A** HEK-293 cells were co-transfected with the indicated plasmids along with pNF-κB-luc plasmids or the control-luciferase plasmid and subjected to a reporter assay. Luciferase assay indicated that RNF2 but not the ΔR mutant induces the activation of NF-κB signaling. **B** Western blot analysis of p-IκBα, IκBα, p-IKKα/β, IKKα, IKKβ, and β-actin in RNF2 KO Hepa1-6 cells or shRNF2 Sk-Hep1 cells. **C** Western blotting analysis of IκBα expression in the indicated cells treated with TNF-α (10 ng/ml) in RNF2 KO Hepa1-6 cells or shRNF2 Sk-Hep1 cells. β-Actin is used as a loading control. **D** Assay of NF-κB luciferase reporter gene activity in RNF2-overexpressing Hepa1-6 or Sk-Hep1 cells transfected with vector or the IκBα dominant-negative mutant (IκBα-mu). Statistics calculated using one-way ANOVA post hoc Tukey test for multi-group or two-tailed Student's t-test for two-group comparisons. $^{**}p < 0.01$

levels in Hepa1-6 and Sk-Hep1 cells (Fig. 5D). Furthermore, ELISA assays consistently revealed that RNF2 deficiency significantly reduced CXCL1 secretion in cell culture supernatants of Hepa1-6 and Sk-Hep1 cells (Fig. 5D). To corroborate these findings in vivo, we examined CXCL1 levels in tumor tissue, tumor lysates, and serum from a syngeneic Hepa1-6 tumor model. RNF2 knockout in Hepa1-6 tumors led to down-regulation of CXCL1 levels in tumor

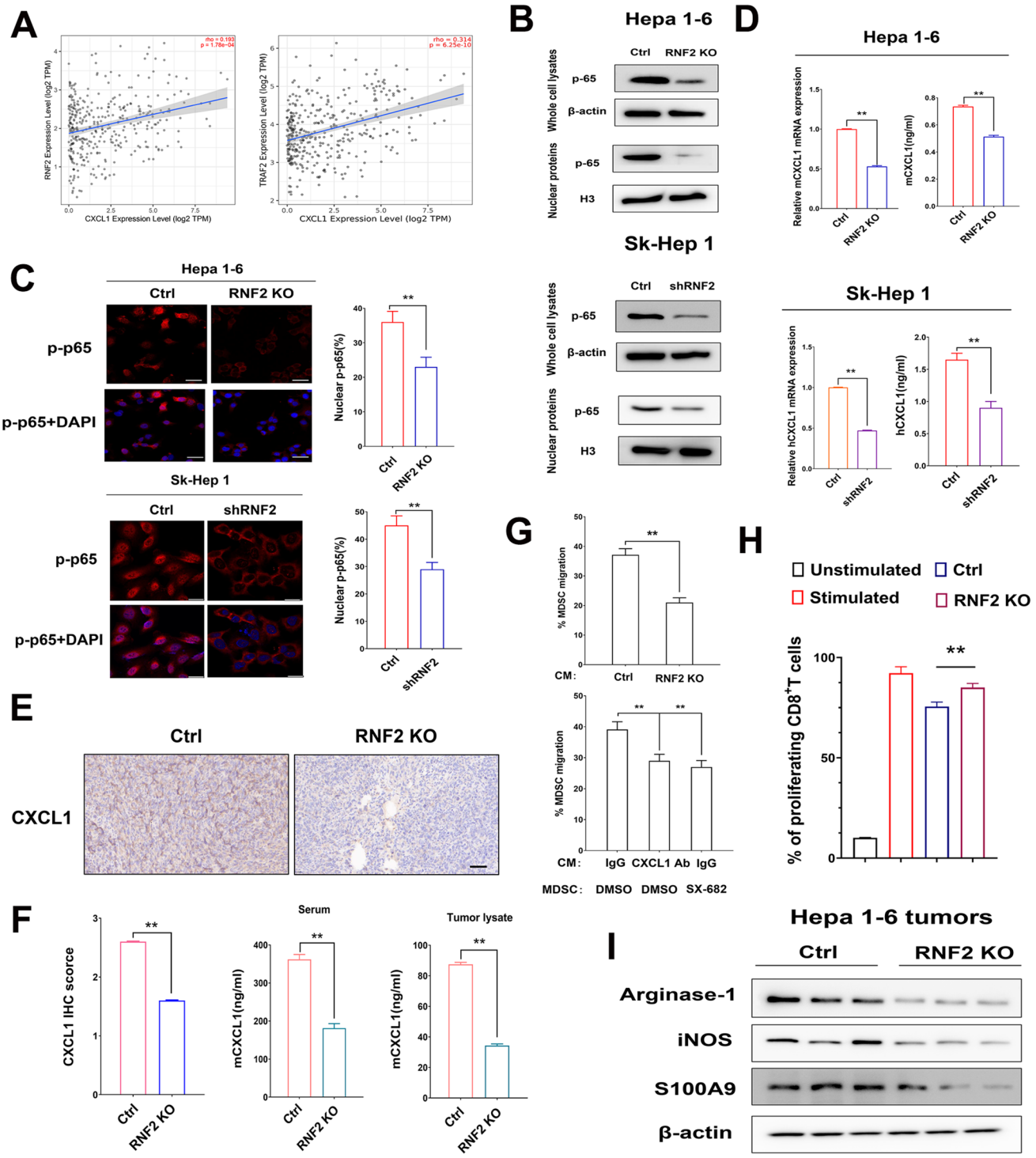

tissue, tumor lysates, and serum (Fig. 5E-5F). In summary, these results suggest that RNF2 in tumor cells induces the activation of the NF-κB pathway, which contributes to the expression of CXCL1.

Since RNF2 knockout reduced MDSC infiltration in the HCC tumor microenvironment, we investigated whether RNF2 regulates MDSC migration via the CXCL1/CXCR2 axis. To investigate whether RNF2 modulates Hepa1-6

◂**Fig. 5** RNF2 induces CXCL1 via the NF-κB pathway **A** Analysis of the TIMER 2.0 database revealed the relationship between RNF2 and CXCL1, as well as TRAF2 and CXCL1, in tumors of patients with liver hepatocellular carcinoma. **B** Western blot analysis was performed to determine the expression of p65 in RNF2 KO Hepa1-6 cells and shRNF2 Sk-Hep1 cells. Whole-cell lysates and nuclear protein extracts were subjected to immunoblotting for p65 levels. **C** Immunofluorescence assays were conducted to detect phosphorylated p65 (p-p65) in RNF2 KO Hepa1-6 cells or shRNF2 Sk-Hep1 cells. DAPI (blue) was used as a nuclear counterstain. Quantification of nuclear p-p65 positive staining in at least 200 counted cells is presented as percentage ± SEM. **D** RT-qPCR analysis was used to assess CXCL1 mRNA expression in RNF2 KO Hepa1-6 cells or shRNF2 Sk-Hep1 cells. ELISA was then performed to validate CXCL1 levels in cell culture supernatants from these cultured cells. (E–F) Representative immunohistochemistry images and quantification of CXCL1 expression in tumor-burdened livers from the Hepa1-6 syngeneic tumor models. ELISA was used to validate CXCL1 levels in tumor lysates and sera from these models. Scale bar represents 50 μm. **G** Migration of MDSCs toward conditioned medium from Hepa1-6 cells (control versus RNF2 KO) were analyzed by transwell MDSC migration assays in triplicate. Migration of MDSCs toward conditioned medium (CM) from Hepa1-6 cells treated with Vehicle or immunoglobulin G (IgG) control, CXCL1-neutralizin antibody, or SX-682 **H** Quantification of the proliferation of CFSE-labeled CD8 + T cells cocultured with MDSCs from tumor-burdened livers of Hepa1-6-Ctrl or Hepa1-6- RNF2 KO tumors, analyzed by flow cytometry. Data are representative of results obtained in three independent experiments. **I** Western blotting analysis of suppressive activity MDSCs from Hepa1-6 syngeneic tumors. Statistics calculated using one-way ANOVA post hoc Tukey test for multi-group or two-tailed Student's t-test for two-group comparisons. $^{**}p < 0.01$.

cell-mediated MDSC recruitment, we first collected conditioned medium from Hepa1-6 cells with or without RNF2 knockout; with or without SX-682 or CXCL1 antibody and then evaluated their ability to induce MDSC migration in a transwell assay. We found that conditioned medium from wild-type Hepa1-6 cells enhanced MDSC migration, which was impaired by the knockout of RNF2. Furthermore, decreased MDSC migration was observed with the addition of the CXCR2 inhibitor SX-682 or anti-CXCL1 neutralizing antibody to conditioned medium derived from Hepa1-6 cells cultures (Fig. 5G). These findings indicate that RNF2 promotes MDSC migration through the CXCL1/CXCR2 axis.

We next assessed whether RNF2 influences MDSC function. MDSCs were isolated from Hepa1-6 syngeneic tumors and then cocultured with T cells in vitro. MDSCs isolated from control tumors suppressed $CD8^+$T cell proliferation. However, MDSCs from RNF2 KO tumors exhibited significantly less suppressive activity against the proliferation of both $CD8^+$T cells compared with MDSCs from the control (Fig. 5H). In support of this, MDSCs isolated from RNF2 KO tumors have reduced expression of MDSC functional markers arginase-1 (Arg1), S100A9, and inducible nitric oxide synthase (iNOS) compared with RNF2 Ctrl tumors (Fig. 5I). Together, these findings confirmed that RNF2 induces MDSC infiltration and an immunosuppressive tumor microenvironment in HCC via the NF-κB-CXCL1 axis.

RNF2 inhibition sensitizes HCC to anti-PD-1 therapy

To further extend the clinical relevance of our study, we sought to apply our findings to predict patient response to anti-PD-1 therapies. Because datasets for HCC patients treated with immune checkpoint blockade are not available, we analyzed publicly available published datasets from melanoma patients treated with anti-PD-1 therapies23. Our analysis revealed that in patients with melanoma, those with low RNF2 expression experienced more favorable survival rates and longer survival times in comparison with patients with high RNF2 expression (Fig. 6A). Additionally, when comparing matched pre- and post-treatment melanoma samples, RNF2 expression significantly decreased following anti-PD-1 therapy.

Anti-PD-1 therapy primarily exerts its anti-tumor effects by enhancing T cell activity. Given that tumor-derived RNF2 promotes immunosuppression by recruiting and activating MDSCs, we hypothesized that combining RNF2 inhibition with anti-PD-1 therapy could enhance therapeutic efficacy. To test this hypothesis, we established subcutaneous HCC mouse models with RNF2 knockout or control cells and treated them with either an anti-PD-1 monoclonal antibody or isotype control. Notably, the combination therapy involving anti-PD-1 and RNF2 knockout resulted in a substantial delay in tumor growth and significant tumor size reduction compared with either monotherapy groups (Fig. 6B-6C).

To further confirm that $CD8^+$T cells and MDSCs infiltrate into tumor tissues after combination therapy with anti-PD-1 and RNF2 knockout, we performed immunohistochemistry staining for tumor-infiltrating $CD8^+$T cells and MDSCs. Histological analyses verified that apart from increasing total $CD8^+$T cells, combining application of RNF2 knockout and anti-PD-1 treatment could also significantly decrease MDSCs infiltration (Fig. 6D). Moreover, RNF2 KO combined with anti-PD-1 synergistically decreased cell proliferation while increased apoptosis (Fig. 6E). Taken together, these results indicated that RNF2 knockout could dampen the immunosuppressive function of MDSCs to promote T cell response, which jointly contributed to the increased sensitivity to anti-PD-1 immunotherapy in HCC mouse models.

Discussion

Tumors employ a range of immunosuppressive strategies to evade anti-tumor immune responses 24. Several alterations in both cancer cells and the tumor microenvironment have been implicated in the failure of immune checkpoint blockade therapy, including a lack of antigenic mutations, T cell exclusion, and the accumulation of immune-suppressive

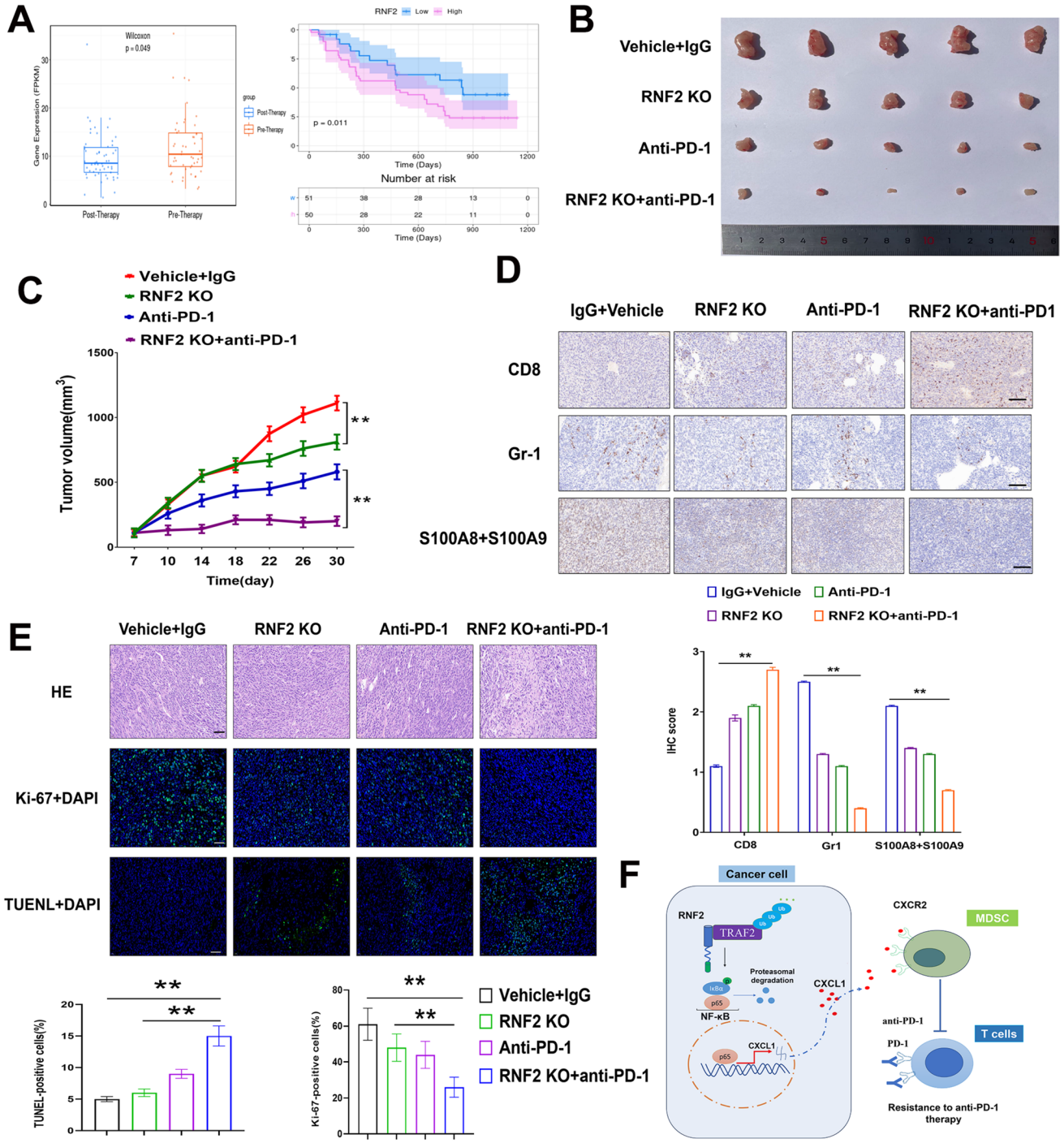

cells25. In this study, we found that RNF2 is significantly upregulated in hepatocellular carcinoma, as evidenced by analysis of the TCGA dataset and clinical samples, and its expression is associated with advanced clinical stages and poor prognosis. Our findings demonstrated that RNF2 is crucial for tumor growth in murine HCC tumor transplantation models. Inhibition of RNF2 significantly suppressed tumor growth. Chemokines, which recruit immune cells to sites of

◂**Fig. 6** RNF2 inhibition sensitizes HCC to anti-PD-1 therapy by recruiting MDSCs into the tumor microenvironment **A** Representative dot plots comparing matched pre- and post-treatment melanoma patient RNF2 mRNA levels in melanoma patients. Statistics calculated using two-sided Wilcoxon matched pair rank test with significance at $p < 0.05$. Kaplan–Meier curves predicting survival of melanoma patients receiving anti-PD-1 therapy based on net changes in RNF2 mRNA levels in the melanoma-GSE91061-anti-PD-1 datasets. (B-C) C57BL/6 J mice were subcutaneously injected with Hepa1-6-Ctrl or Hepa1-6-RNF2 KO cells and treated with either anti-PD-1 or isotype control. Tumor growth was monitored until the experimental endpoints, with data presented as mean ± SEM. Tumor growth curves are shown. **D** Representative images of IHC for CD8, Gr1, and S100A8 + S100A9 in indicated mouse tumors and IHC quantification. The scale bars represent 50 μm. **E** Representative H&E staining (upper), immunostaining and quantification of Ki-67- and TUNEL-positive cells (lower). The scale bars represent 50 μm. **F** A schematic diagram illustrates the RNF2-TRAF2-CXCL1 axis driving MDSC accumulation, leading to suppression of T cell function in HCC. High RNF2 expression is positively correlated with MDSC infiltration in HCC patients. RNF2 enhances NF-κB activation by regulating K63-linked ubiquitination of TRAF2, resulting in elevated CXCL1 expression, a chemoattractant for MDSCs via the CXCL1-CXCR2 axis. RNF2-recruited MDSCs inhibit the activity of effector CD8 + T cells within the tumor immune microenvironment, thereby promoting immunosuppression and tumor progression in HCC. Statistics calculated using one-way ANOVA post hoc Tukey test for multi-group or two-tailed Student's t-test for two-group comparisons. $^{**}p < 0.01$

inflammation, contribute to the pathogenesis of HCC 26. We propose that tumor-derived RNF2 enhances the recruitment of MDSC via the CXCL1-CXCR2 axis, thereby inhibiting the anti-tumor immune response. Furthermore, our analysis of anti-PD-1 responses suggests that RNF2 may serve as a predictive biomarker for identifying responders to anti-PD-1 therapy. Collectively, our findings support the potential of targeting RNF2 and MDSCs as therapeutic strategies for HCC.

The tumor microenvironment consists of not only a heterogeneous population of tumor cells but also various resident and infiltrating stroma cells, immune cells, secreted cytokines, and extracellular matrix proteins27, 28. The interactions between tumor cells and immune cells, along with cytokine signaling, play a critical role in determining the progression of tumors 27. Tumor cells employ multiple mechanisms to escape T cell immune surveillance and promote their own growth. MDSCs, a heterogeneous population consisting of monocytic and granulocytic cells, exert a variety of immunosuppressive effects29. Both MDSCs and regulatory T cells can be induced to shift the immune balance toward T cell suppression 30. In this study, we identified an important link between RNF2 expression and the recruitment of MDSCs to tumors, revealing a novel pathway through which RNF2 mediates immunosuppression. Notably, we observed an increase in tumor-infiltrating MDSCs with potent immunosuppressive activity in the HCC tumor model. These findings indicate that RNF2 expression in tumors not only drives the recruitment of the MDSC population but also imparts suppressive properties to these cells.

TRAF2 functions as a signaling adaptor protein that links upstream stimuli, such as TNFR signaling, to downstream effectors involved in NF-κB activation. The stability and activity of TRAF2 are regulated by various post-translational modifications, including ubiquitination. In particular, K63-linked polyubiquitination of TRAF2 is pivotal for forming the signaling complex or "signalosome" that facilitates the recruitment and activation of TAK1. TAK1 then phosphorylates the IκB kinase complex, which, in turn, leads to the phosphorylation and degradation of IκB proteins 31. This degradation releases NF-κB dimers, allowing them to translocate into the nucleus and activate target gene transcription, promoting cell survival, proliferation, and inflammatory responses 7. In our current study, we found that RNF2 binds to TRAF2 and promotes its K63-linked ubiquitination. Mutations in the TRAF2 ΔRING domain abolished the K63-linked ubiquitination of TRAF2 and disrupted RNF2-induced NF-κB signaling activation, suggesting that the importance of this modification in maintaining NF-κB activation. Given that TRAF2 is essential for NF-κB signalosome formation, disrupting its activity through the inhibition of RNF2 could be a promising strategy to inhibit NF-κB signaling in tumors. In the current study, we found that RNF2 knockout mitigates the immunosuppressive activity of MDSCs, thereby enhancing T cell responses, which jointly contributed to the increased sensitivity to anti-PD-1 immunotherapy in HCC mouse models. Therefore, combining RNF2 inhibition with immune checkpoint inhibitors, such as anti-PD-1 therapy, could further enhance anti-tumor immunity by alleviating the immunosuppressive effects of NF-κB activation in the tumor microenvironment.

Proinflammatory cytokines within the tumor microenvironment play a critical role in suppressing anti-tumor immunity while promoting tumor cell survival32–34. Understanding the intricate crosstalk between cancer cells and the immune system during inflammation is essential for enhancing immune-based therapies, particularly in inflammation-driven malignancies such as breast, liver, and colorectal cancers 9, 32, 35, 36. A key driver of this process is the activation of the classical NF-κB signaling pathway, which has been shown to impede the efficacy of immunotherapies 11. In tumor cells, NF-κB activation, particularly via TNF signaling, upregulates the expression of proinflammatory cytokines and chemokines, establishing a feedback loop

between NF-κB in both tumor and stromal cells that perpetuates immune suppression, especially in hepatocellular carcinoma9, 20. One of the downstream targets of NF-κB is CXCL1, a chemokine that plays a pivotal role in recruiting MDSCs to the tumor microenvironment by engaging the CXCR2 receptor, thereby promoting an immunosuppressive milieu 21. Our research demonstrated that inhibition of RNF2 significantly reduces CXCL1 mRNA expression and secretion in both murine and human HCC cell lines. This repression of CXCL1 correlates with diminished MDSC recruitment, as RNF2 promotes MDSC recruitment by enhancing CXCL1-CXCR2 signaling. These findings suggest that RNF2-mediated NF-κB signaling orchestrates a critical immunosuppressive network by enhancing MDSC infiltration via CXCL1 secretion, identifying RNF2 as a potential therapeutic target to disrupt immune evasion in HCC.

Conclusions

In summary, our results indicated that RNF2 plays a pivotal role in the progression of HCC by fostering an immunosuppressive microenvironment and promoting resistance to immune checkpoint blockade therapy. Through its interaction with TRAF2 and subsequent activation of the NF-κB signaling pathway, RNF2 drives the recruitment of MDSCs, which inhibit T cell activation and support tumor growth (Fig. 6F). By elucidating the regulation of MDSC recruitment and function by RNF2, our study provides valuable insights into the link between RNF2 signaling and the development of the immunosuppressive tumor microenvironment, opening new avenues for therapeutic intervention.

Supplementary Information The online version contains supplementary material available at https://doi.org/10.1007/s00262-025-04002-6.

Author contributions Manman Liang, Yufeng Gao, and Biao Geng designed the study, analyzed the data, and wrote the manuscript. Manman Liang, Jianghua Yang, and Aiping Zhang performed most of the experiments. Na Zhong, Bin Quan, Zijian Wang, and Wenying Zhao assisted with the generation of reagents and analysis of data. All authors provided critical feedback on the manuscript. All authors read and approved the final manuscript.

Funding This work received support from various sources, including grants from the National Natural Science Foundation of China (82370608;82204458), Natural Science Foundation of Anhui Province (2208085MH204), Natural Science Foundation of Education Department of Anhui Province (2022AH040160; 2023AH040266), Anhui Provincial Special Fund for Clinical Medical Research Transformation (202304295107020040).

Data availability No datasets were generated or analyzed during the current study.

Declarations

Competing interests The authors declare no competing interests.

Ethics approval All patients authorized the use of their specimens by written informed consent. The protocols used in our study were approved by the Ethics Committee of Yijishan Hospital. All animal experiments were approved by the Animal Care Committee of Yijishan Hospital.

Consent for publication All authors agree for publication.

References

1. Liu T, Meng G, Ma S, You J, Yu L, He R, Zhao X, Cui Y (2024) Progress of immune checkpoint inhibitors in the treatment of advanced hepatocellular carcinoma. Front Immunol 15:1455716
2. Hao L, Li S, Ye F, Wang H, Zhong Y, Zhang X, Hu X, Huang X (2024) The current status and future of targeted-immune combination for hepatocellular carcinoma. Front Immunol 15:1418965
3. Kumar V, Patel S, Tcyganov E, Gabrilovich DI (2016) The Nature of Myeloid-Derived Suppressor Cells in the Tumor Microenvironment. Trends Immunol 37:208–220
4. Kalathil SG, Thanavala Y (2021) Importance of myeloid derived suppressor cells in cancer from a biomarker perspective. Cell Immunol 361:104280
5. Ma C, Zhang Q, Greten TF (2021) MDSCs in liver cancer: A critical tumor-promoting player and a potential therapeutic target. Cell Immunol 361:104295
6. Lu J, Luo Y, Rao D, Wang T, Lei Z, Chen X, Zhang B, Li Y, Liu B, Xia L, Huang W (2024) Myeloid-derived suppressor cells in cancer: therapeutic targets to overcome tumor immune evasion. Exp Hematol Oncol 13:39
7. Wang S, He Y, Wang J, Luo E (2024) Re-exploration of immunotherapy targeting EMT of hepatocellular carcinoma: Starting from the NF-kappaB pathway. Biomed Pharmacother 174:116566
8. Jayachandran A, Dhungel B, Steel JC (2016) Epithelial-to-mesenchymal plasticity of cancer stem cells: therapeutic targets in hepatocellular carcinoma. J Hematol Oncol 9:74
9. Y. Grinberg-Bleyer, H. Oh, A. Desrichard, D.M. Bhatt, R. Caron, T.A. Chan, R.M. Schmid, U. Klein, M.S. Hayden, S. Ghosh,

NF-kappaB c-Rel Is Crucial for the Regulatory T Cell Immune Checkpoint in Cancer, Cell, 170 (2017) 1096–1108 e1013.
10. Li A, Jacks T (2017) Driving Rel-iant Tregs toward an Identity Crisis. Immunity 47:391–393
11. Grinberg-Bleyer Y, Caron R, Seeley JJ, De Silva NS, Schindler CW, Hayden MS, Klein U, Ghosh S (2018) The Alternative NF-kappaB Pathway in Regulatory T Cell Homeostasis and Suppressive Function. J Immunol 200:2362–2371
12. Liang M, Sun Z, Chen X, Wang L, Wang H, Qin L, Zhao W, Geng B (2023) E3 ligase TRIM28 promotes anti-PD-1 resistance in non-small cell lung cancer by enhancing the recruitment of myeloid-derived suppressor cells. J Exp Clin Cancer Res 42:275
13. T. Li, J. Fu, Z. Zeng, D. Cohen, J. Li, Q. Chen, B. Li, X.S. Liu, TIMER2.0 for analysis of tumor-infiltrating immune cells, Nucleic Acids Res, 48 (2020) W509-W514.
14. Newman AM, Liu CL, Green MR, Gentles AJ, Feng W, Xu Y, Hoang CD, Diehn M, Alizadeh AA (2015) Robust enumeration of cell subsets from tissue expression profiles. Nat Methods 12:453–457
15. Finotello F, Mayer C, Plattner C, Laschober G, Rieder D, Hackl H, Krogsdam A, Loncova Z, Posch W, Wilflingseder D, Sopper S, Ijsselsteijn M, Brouwer TP, Johnson D, Xu Y, Wang Y, Sanders ME, Estrada MV, Ericsson-Gonzalez P, Charoentong P, Balko J, de Miranda N, Trajanoski Z (2019) Molecular and pharmacological modulators of the tumor immune contexture revealed by deconvolution of RNA-seq data. Genome Med 11:34
16. Aran D, Hu Z, Butte AJ (2017) xCell: digitally portraying the tissue cellular heterogeneity landscape. Genome Biol 18:220
17. Becht E, Giraldo NA, Lacroix L, Buttard B, Elarouci N, Petitprez F, Selves J, Laurent-Puig P, Sautes-Fridman C, Fridman WH, de Reynies A (2016) Estimating the population abundance of tissue-infiltrating immune and stromal cell populations using gene expression. Genome Biol 17:218
18. J. Racle, K. de Jonge, P. Baumgaertner, D.E. Speiser, D. Gfeller, Simultaneous enumeration of cancer and immune cell types from bulk tumor gene expression data, Elife, 6 (2017).
19. Cao Q, Wang X, Zhao M, Yang R, Malik R, Qiao Y, Poliakov A, Yocum AK, Li Y, Chen W, Cao X, Jiang X, Dahiya A, Harris C, Feng FY, Kalantry S, Qin ZS, Dhanasekaran SM, Chinnaiyan AM (2014) The central role of EED in the orchestration of polycomb group complexes. Nat Commun 5:3127
20. Guo Q, Jin Y, Chen X, Ye X, Shen X, Lin M, Zeng C, Zhou T, Zhang J (2024) NF-kappaB in biology and targeted therapy: new insights and translational implications. Signal Transduct Target Ther 9:53
21. Eluard B, Thieblemont C, Baud V (2020) NF-kappaB in the New Era of Cancer Therapy, Trends. Cancer 6:677–687
22. J. Korbecki, K. Barczak, I. Gutowska, D. Chlubek, I. Baranowska-Bosiacka, CXCL1: Gene, Promoter, Regulation of Expression, mRNA Stability, Regulation of Activity in the Intercellular Space, Int J Mol Sci, 23 (2022).
23. N. Riaz, J.J. Havel, V. Makarov, A. Desrichard, W.J. Urba, J.S. Sims, F.S. Hodi, S. Martin-Algarra, R. Mandal, W.H. Sharfman, S. Bhatia, W.J. Hwu, T.F. Gajewski, C.L. Slingluff, Jr., D. Chowell, S.M. Kendall, H. Chang, R. Shah, F. Kuo, L.G.T. Morris, J.W. Sidhom, J.P. Schneck, C.E. Horak, N. Weinhold, T.A. Chan, Tumor and Microenvironment Evolution during Immunotherapy with Nivolumab, Cell, 171 (2017) 934–949 e916.
24. Xia X, Yang Z, Lu Q, Liu Z, Wang L, Du J, Li Y, Yang DH, Wu S (2024) Reshaping the tumor immune microenvironment to improve CAR-T cell-based cancer immunotherapy. Mol Cancer 23:175
25. Chen Y, Liu Y, Han L (2023) Spatial landscape of the tumor immune microenvironment, Trends. Cancer 9:459–460
26. Ruishi X, Linyi X, Yunfan B, Wenbo Y, Xiaoying Z, Xiaoxue F, Difu Z, Xintian L, Ming Z, Haoming L (2024) New perspectives on chemokines in hepatocellular carcinoma therapy: a critical pathway for natural products regulation of the tumor microenvironment. Front Immunol 15:1456405
27. Yin Y, Feng W, Chen J, Chen X, Wang G, Wang S, Xu X, Nie Y, Fan D, Wu K, Xia L (2024) Immunosuppressive tumor microenvironment in the progression, metastasis, and therapy of hepatocellular carcinoma: from bench to bedside. Exp Hematol Oncol 13:72
28. Chen C, Wang Z, Ding Y, Qin Y (2023) Tumor microenvironment-mediated immune evasion in hepatocellular carcinoma. Front Immunol 14:1133308
29. A. Argentiero, A. Delvecchio, R. Fasano, A. Andriano, I.C. Caradonna, R. Memeo, V. Desantis, The Complexity of the Tumor Microenvironment in Hepatocellular Carcinoma and Emerging Therapeutic Developments, J Clin Med, 12 (2023).
30. Zhou Z, Hu Y, Wu Y, Qi Q, Wang J, Chen L, Wang F (2022) The immunosuppressive tumor microenvironment in hepatocellular carcinoma-current situation and outlook. Mol Immunol 151:218–230
31. R. Gupta, M.M. Kadhim, A. Turki Jalil, A.M. Obayes, Z. Aminov, F. Alsaikhan, A.A. Ramirez-Coronel, P. Ramaiah, N.A. Tayyib, X. Luo, Multifaceted role of NF-kappaB in hepatocellular carcinoma therapy: Molecular landscape, therapeutic compounds and nanomaterial approaches, Environ Res, 228 (2023) 115767.
32. Rossari F, Birocchi F, Naldini L, Coltella N (2023) Gene-based delivery of immune-activating cytokines for cancer treatment. Trends Mol Med 29:329–342
33. Baker RG, Hayden MS, Ghosh S (2011) NF-kappaB, inflammation, and metabolic disease. Cell Metab 13:11–22
34. Gu M, Zhou X, Sohn JH, Zhu L, Jie Z, Yang JY, Zheng X, Xie X, Yang J, Shi Y, Brightbill HD, Kim JB, Wang J, Cheng X, Sun SC (2021) NF-kappaB-inducing kinase maintains T cell metabolic fitness in antitumor immunity. Nat Immunol 22:193–204
35. Capece D, Verzella D, Flati I, Arboretto P, Cornice J, Franzoso G (2022) NF-kappaB: blending metabolism, immunity, and inflammation. Trends Immunol 43:757–775
36. Catrysse L, van Loo G (2017) Inflammation and the metabolic syndrome: the tissue-specific functions of NF-kappaB. Trends Cell Biol 27:417–429